ADVANCED FUNCTIONAL MATERIALS
www.afm-journal.de



# Recombination Through Different Types of Localized States in Organic Solar Cells

*Robert A. Street,* Alexa Krakaris, and Sarah R. Cowan*

**Recombination in bulk heterojunction solar cells is explored by observing the result of prolonged white light illumination, thermal annealing to high temperature, and chemical doping. Measurements of the photocurrent spectral response, the steady state photocurrent-voltage characteristics, transient photoconductivity and the dark forward bias current on polymer:fullerene solar cells provide information about the density of states and the electronic properties. Illumination generates deep localized states in the interface gap, which act as recombination centers and also increase the diode ideality factor. Annealing induces both nanostructural and electronic changes. The coarsening of the domain structure reduces the probability that excitons reach the interfaces and also reduces the charge transfer absorption. At the same time annealing broadens the exponential band tails and increases the recombination rate. Doping introduces shallow states near the fullerene conduction band, which also act as recombination centers. The results show that recombination is through localized states of different character, depending on the circumstances.**

## 1. Introduction

Until recently it was widely thought that geminate and/or Langevin (bimolecular) recombination were the dominant mechanisms that limit the performance of organic bulk heterojunction (BJH) solar cells.[1–4] In 2010 we pointed out that the cell data for poly(carbazole-dithienyl-benzothiadiazole):phenyl $C_{70}$-butyric acid methyl ester (PCDTBT:$PC_{70}$BM) and poly(3-hexylthiophene)(P3HT):$PC_{60}$BM suggested the importance of recombination through localized states, which is a common mechanism in disordered materials.[5] The Shockley-Read-Hall-type recombination model accounts for the current–voltage characteristics and is supported by the form of the dark forward bias data, having a diode ideality factor substantially greater than 1. Subsequently, a specific experimental test showed that geminate recombination was not a significant channel in either type of solar cell.[6]

Dr. R. A. Street, A. Krakaris
Palo Alto Research Center, 3333 Coyote Hill Road
Palo Alto, CA 94304, USA
E-mail: street@parc.com
Dr. S. R. Cowan
Center for Polymers and Organic Solids
University of California at Santa Barbara
Santa Barbara, CA 93106, USA

DOI: 10.1002/adfm.201200031

Various experiments confirm that localized states within the band gap are present in organic solar cells, in the form of an exponential distribution of band tail states and a broader distribution of deeper localized states.[7–14] In particular, Beiley et al.[11] show evidence for an exponential band tail of traps in PCDTBT:PCBM and Shuttle et al.[12] use transient photoconductivity to demonstrate the presence of deep traps in a different polymer. Together these studies lead to a description of electronic transport in which carriers move at a more or less well defined transport energy where the density of states is high enough for rapid hopping, The band tail and deeper localized states act as traps, in the sense that carriers in these states must be thermally excited to higher energy mobile states in order to move because the density of states is too low for significant hopping.

These localized trap states are obvious candidates for recombination centers. Recombination centers are of necessity located near the heterojunction interface so that they are accessible by both holes in the donor and electrons in the acceptor. If the traps are located randomly within the materials then only a subset near the interface will be recombination centers. The spatial distribution of traps is discussed later in the paper.

This paper describes alternative techniques used to modify the localized trap state distribution making it possible to relate the changes in state density to the changes in the cell recombination and electronic transport. Our studies demonstrate a correlation between the presence of localized states and the magnitude of the recombination. The data also show that different types of localized states can be involved in recombination, depending on the circumstances. Three methods of changing the localized state distribution are studied; exposure to prolonged illumination, thermal annealing up to the cell melting temperature and chemical doping. In each case the cells are degraded in performance from the pristine state, in part due to an increase in the density of recombination centers.

In order to deduce the specific cause of the changes in the solar cell characteristics, it is necessary to have detailed information about the electronic structure and about the transport and recombination mechanisms that apply. Our recent studies have shown that the measurement of the photocurrent spectral response and the transient photoconductivity combine to characterize the density of states (DOS) distribution and the transport processes.[11,12] These experiments together with

theoretical calculations of the band edge DOS provide a quantitative measurement of the exponential band tails near the band edges and the broader distribution of deeper states across the band gap. Spectral response measurements are used in this paper to characterize and quantify the density of states, while steady state photocurrent and dark forward bias current measurements provide complementary information about the recombination.

The paper has three goals. The first goal is to explore the experimental evidence that localized states provide the dominant recombination mechanism in BJH cells. The second goal is to show how the various electronic measurements are all connected to the recombination mechanisms. The third goal is to use these experimental techniques to quantify the changes in the density and type of localized states as a result of the structural changes induced by light exposure, annealing environmental exposure etc.

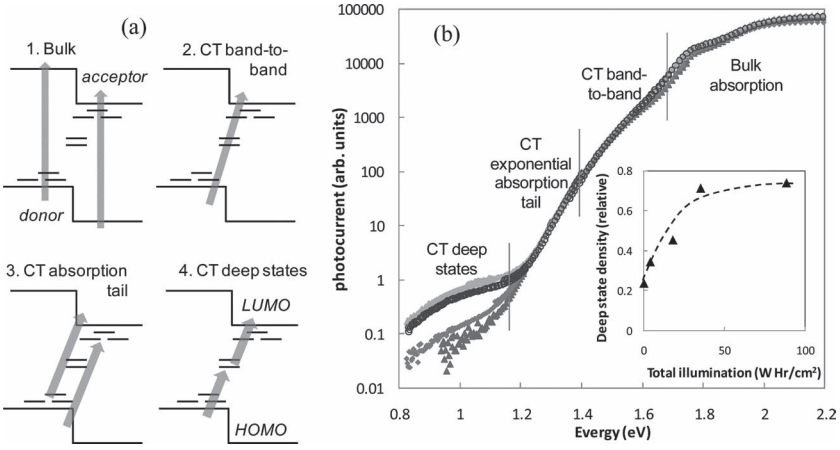


**Figure 1.** a) Illustration of the different optical transitions that can excite photoconductive carriers in a BHJ solar cell. Lines indicate the HOMO and LUMO levels of the donor and acceptor materials and short lines represent band tail or deep localized states. b) Examples of the spectral response of PCDTBT:PCBM after increasing amounts of white light illumination, showing the increase in response between 0.8 and 1.2 eV. The four types of optical transitions are indicated. The inset shows the deep state density as measured by the low energy response versus the total white light exposure.

## 2. Results

All the experiments are performed on PCDTBT:PCBM solar cells, and their fabrication is described elsewhere.[13] The doped samples described in Section 2.4 are fabricated with $PC_{60}BM$, while the other samples are fabricated with $PC_{70}BM$. The samples are protected with a glass cover slip secured with UV-cured epoxy, which slows the absorption of gases from the ambient. The samples were stored in nitrogen when not being measured or processed.

### 2.1. Experimental Methodology

The photocurrent spectral response is measured to observe changes in the optical absorption processes, the voltage dependence of the dark and photocurrent to monitor charge collection, and in some cases transient photoconductivity is used to measure the changes in carrier mobility.

Spectral response is a measurement of the cell photocurrent as a function of excitation photon energy. In effect, this experiment measures the optical absorption arising from those transitions that create mobile carriers. The photoconductivity spectral response measured at a bias voltage V can be described by,

$$J_{PC}(E_{PH}, V) = G A_B(E_{PH})\, P_X P_C(V) \quad (1)$$

$G$ is the incident light intensity, $A_B(E_{PH})$ is the optical absorption at photon energy $E_{PH}$, $P_X$ is the probability that an absorbed photon creates an electron-hole pair at the interface and each of these parameters are independent of the applied bias voltage $V$. $P_C(V)$ is the probability of charge collection of the separated carriers, and will have a different form depending on the specific recombination mechanism.

The primary interest in the spectral response is the optical absorption measurement and the information it provides about the density of states distribution. There are four regions of interest in the typical measurement of a BHJ cell, illustrated in **Figure 1**a. The highest energy region corresponds to bulk absorption in the polymer and fullerene, while the lower energy region corresponds to direct excitation from the highest occupied molecular orbital (HOMO) of the polymer to the lowest unoccupied molecular orbital (LUMO) of the fullerene across the interface band gap. Absorption of this type is often referred to as charge transfer (CT) excitation; this form of absorption occurs below about 1.7 eV for PCDTBT:PCBM, with the bulk absorption dominating at higher energy. Within the CT excitations there are band-to-band transitions above about 1.4 eV, an exponential absorption tail from about 1.1 eV to 1.4 eV, and deep state transitions below about 1.1 eV.[14] Previous studies have shown that the exponential absorption tail provides a quantitative measurement of the corresponding exponential band tail of localized states in the polymer valence band density of states.[15] The spectral response data therefore provides all of the characteristic features of the density of states distribution. Lee et al. have confirmed that the spectral response is an accurate measure of the CT optical absorption.[16] Vandewal et al. also concluded that the spectral response measures the CT absorption but analyze it using a different model from ours.[17]

The steady state photocurrent $J_{PC}(V)$ is the difference between the current under illumination and in the dark and its form directly relates to the recombination processes. Here $J_{PC}(V)$ is analyzed using the charge collection model introduced previously,[5]

$$J_{PC}(V) = J_{MAX} S(V_{BI} - V) \times \left(1 - \exp\left[-\frac{1}{S(V_{BI} - V)}\right]\right); \quad S = \mu\tau / dd' \quad (2)$$

$V_{BI}$ is the built-in potential and $J_{MAX}$ is the current at full charge collection which is expected to occur at sufficiently large reverse bias; hence $P_C(V) = J_{PC}(V)/J_{MAX}$. d is the sample thickness and $d'$ ($\sim d/2$) is the average distance a carrier travels to the collection electrode. This expression describes the relative probability of charge collection at the electrode and of recombination. The shape of $J_{PC}(V)$ depends on the mobility-lifetime product $\mu\tau$ and Equation 2 applies to first order recombination mechanisms for which $S$, and hence $\mu\tau$, are independent of illumination intensity. We refer to $S$ as the charge collection parameter.

For the light-induced and thermal annealing changes, $P_C(V)$ and the derived value of $S$ are independent of illumination intensity, demonstrating first order recombination kinetics. However there is a pronounced dependence on light intensity for the doping-induced effects, indicating the presence of a higher order recombination mechanism. In this case the extension of Equation 2 is complicated and instead we apply a simpler model defined by,[18]

$$G = P_F N + P_S N^2 + P_T N (V_{BI} - V);$$
$$J_{PC}(V) = -P_T N (V_{BI} - V)/G \quad (3)$$

$N$ is the carrier concentration, $P_F$, $P_S$ and $P_T$ are the rate constants for first order recombination, second order recombination and charge collection, which is proportional to the internal voltage. The solution of Equation 3 for first order recombination is only slightly different in form from Equation 2.

The dark current is described by the diode equation,[19]

$$J_D(V) = J_0 \left[ \exp\left( \frac{e(V - J_D(V) R_S)}{nkT} \right) - 1 \right] + \frac{V}{R_P} \quad (4)$$

$R_S$ and $R_P$ are the series and parallel (shunt) resistances and $R_S$ is small enough not to need inclusion in the shunt term. The ideality factor n is 1.5 or larger in most organic BHJ cells. Theory tells us that the value of n depends on the recombination mechanism.[20] An earlier publication noted that a large value of $n$ is evidence for localized state recombination, because band-to-band recombination gives $n = 1$, at least for low bias voltages.[5] The relation between $n$ and the recombination center density therefore provides information about the role of traps in the dark current.

### 2.2. Light Exposure of PCDTBT:PCBM

Prolonged light exposure is known to cause degradation in some BHJ solar cells. Reese et al. observe light induced oxidation of PCBM in P3HT:PCBM solar cells,[21] and similar oxidation is observed in other BHJ cells.[22] PCDTBT:PCBM solar cells are reported to have an initial relatively quick degradation under illumination followed by longer term stability.[23] Degradation of the contacts and other layers of the cells, in addition to the active layer, is also observed.[24]

PCDTBT:PCBM solar cells were exposed to white light for an extended time. Figure 1b shows the spectral response after various stages of exposure. The spectra are normalized to the same peak response at about 2.1 eV. With increased total light exposure the peak in the spectral response decreases by about a factor 1.5, mainly due to the charge collection factor $P_C(V)$ in Equation 1. Since the spectral response data are measured at short circuit ($V = 0$), the spectral response is reduced by a factor $P_C(0) = J_{PC}(0)/J_{MAX}$ (see Equation 2) and this value is obtained experimentally from the fit to $J_{PC}(V)$. There are also smaller changes in the absolute magnitude of the spectral response due to small variations of the alignment of the sample to the monochromatic light source.

Figure 1b shows that the only significant change in the spectral response is in the energy region from 0.8 to 1.2 eV and here the broad low energy absorption band increases in strength by about a factor 10. No detectable change is observed in either the above gap CT absorption or the band tails. The inset to Figure 1b shows that the deep state density, as measured by the strength of the spectral response at 1 eV, increases with total light exposure and then saturates. Since the shape of the deep state absorption band is unchanged within experimental uncertainty, the value at 1 eV is an appropriate measure of the relative deep state density. Goris et al. have reported a similar enhancement of the low energy spectral response in P3HT:PCBM exposed to UV light.[25]

**Figure 2** shows examples of the bias dependence of the photocurrent following increasing total illumination exposure. The changing shape of $J_{PC}(V)$ clearly indicates that light exposure increases recombination with a corresponding decrease in solar cell efficiency. The points are the measured data and the lines are fits to the charge collection model of Equation 2, from which the charge collection parameter $S$ is obtained. Furthermore, the form of $J_{PC}(V)$ is independent of illumination intensity indicating first order recombination. The value of $S$ obtained by fitting the $J_{PC}(V)$ data changes by less than 10% over a factor 100 change in light intensity. After the longest light exposure the increased series resistance influences $J_{PC}(V)$ and leads to a slight reduction in $S$ at high light intensity, which can be corrected for.[26]

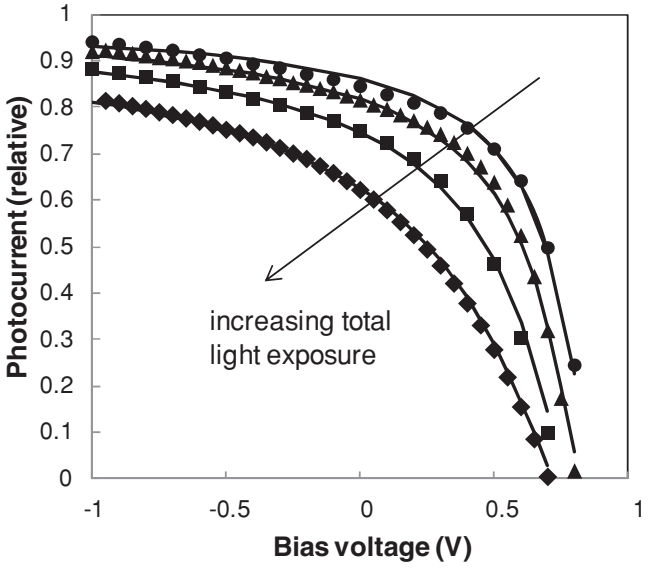


**Figure 2.** Steady state photocurrent, $J_{PC}(V)$ measured after different amounts of total white light exposure. Points are data and the solid lines are fits to Equation 2.

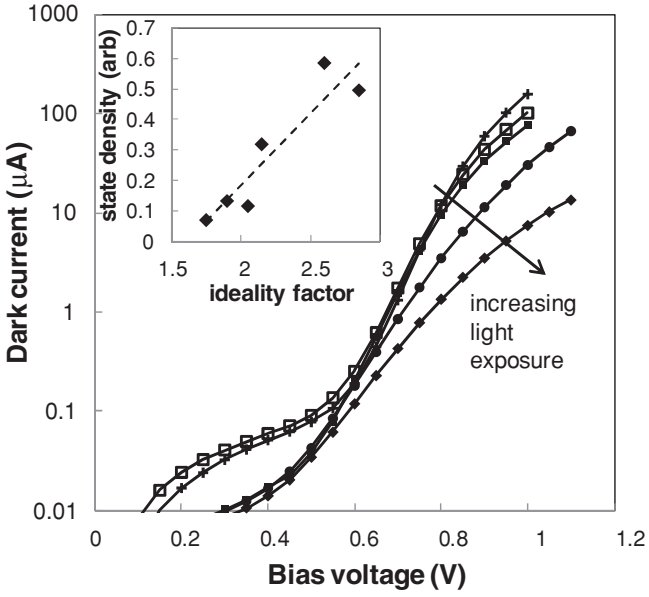


**Figure 3.** Dark forward bias current-voltage characteristics measured after increasing total white light exposure. Points are data and the lines are fits to Equation 4. The inset shows the ideality factor plotted versus the density of deep states obtained from the spectral response data.

The dark current also changes after prolonged light exposure, as shown in **Figure 3**. The lines are fitted to Equation 4 and the ideality factor increases from about 1.7 to above 2.5 as the total light exposure increases. The data also show that both the series resistance and the shunt resistance increase with light exposure. The variation in ideality factor with the deep state density as measured by the spectral response at 1 eV is shown in the inset to Figure 3. Evidently the increase in dark ideality factor is correlated to the increasing deep state density.

### *2.2.1. Recombination Centers Resulting from Light Exposure*

The white light exposure data are relatively straightforward to understand. There is an increase in the density of deep localized states and a corresponding decrease in the charge collection parameter S, which indicates an increase in the recombination centers. The spectral response shows no change in the bulk, the CT band-to-band transitions or the CT absorption tail regions. Hence we conclude that the only change in the electronic structure is the increase in the density of deep states, and that there is no other plausible explanation of the increased recombination.

The onset of the deep state absorption occurs at a photon energy of no more than 0.8 eV, compared to the interface band gap which is at about 1.4 eV (see Figure 1b). Hence the states that correspond to the absorption must extend at least to 0.6 eV from the band edges. Evidently these are states that are much deeper than the band tails. We conclude that the recombination centers are localized states distributed near the center of the interface band gap.

The mobility-lifetime μτ product is related to the density of recombination centers $N_R$. $\mu\tau F$ is the average drift distance carriers move before recombnation, where $F$ is the electric field. The drift distance is inversely proportion to the recombination center density,[27] irrespective of whether the carriers can be considered ballistic or diffusive, hence

$$S \propto \mu\tau = const/\sigma N_R \tag{5}$$

where $\sigma$ is the capture cross section and the constant depends on the details of the transport process. Hence $1/S$ is proportional to the recombination center density. In a situation where there are two (or more) different types of recombination centers, one of which varies with a process parameter $x$, then,

$$\frac{1}{S(x)} = \frac{\sigma_1 N_{R1}(x)}{c_1} + \frac{\sigma_2 N_{R2}}{c_2} \tag{6}$$

where the subscripts 1 and 2 refer to the different recombination centers. Recombination through states that do not vary with the parameter $x$ provide a constant additive term in Equation 6.

**Figure 4** is a plot of the deep trap density obtained from the spectral response as measured by the relative absorption at 1 eV, versus the recombination center density as determined from the value of $1/S$ according to Equation 5 or 6. A linear relation is observed, indicating a direct correlation between the two measurements. The residual value of $1/S$ when the deep state density is zero represents a second recombination channel according to Equation 6 and is discussed further below. The magnitude of the capture cross section cannot be determined since the experiments provide relative rather than absolute values of the deep state density.

The saturation of the light-induced effect in the spectral response is consistent with other measurements of the lifetime of PCDTBT:PCBM solar cells which find an initial drop in cell efficiency followed by stabilization.[23] The data provide no further information about the nature of the deep states, which could be intrinsic to the materials, or related to impurities either in the starting material or atmospheric impurities that

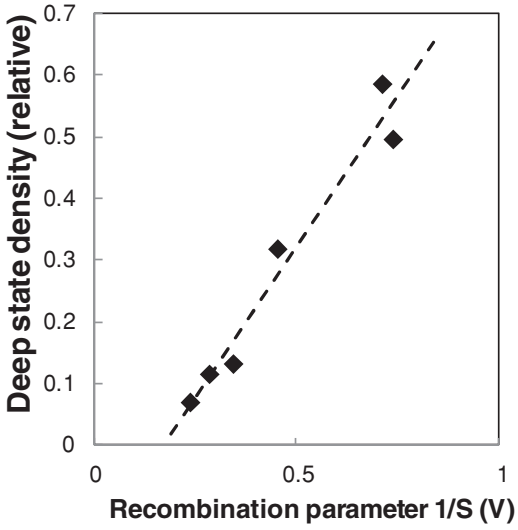


**Figure 4.** Plot of the deep state density measured from the absorption at 1 eV versus the recombination center parameter ($1/S$) derived from the fits of $J_{PC}(V)$ using Equation 2.

diffuse in during the time that the sample is exposed to air Also undetermined is whether the deep states introduced by illumination are at the domain interfaces or uniformly in one or both materials. Only those states that are close enough to the domain interface can act as recombination centers as they need to be accessible to both electrons in the PCBM and holes in the polymer. It seems to us most likely that the deep states are introduced uniformly in one or both materials, but this must be determined by further experiments.

The changes in the forward diode current (Figure 3), correlate the increase in deep trap density to an increase in the ideality factor. This result confirms that the diode dark characteristics reflect the trap density and hence are broadly described by the Shockley-Read Hall generation-recombination mechanism. The effect of deep states increasing the ideality factor, even to values much greater than 2, is known from studies of hydrogenated amorphous silicon which show qualitatively similar changes.[28] The origin of the increasing series resistance is less clear, whether it is also due to the increasing deep trap density in the BHJ structure or a separate light-induced effect on one of the contacts, such as the PEDOT layer. We find that the series resistance continues to increase after the density of recombination centers has saturated, suggesting a contact effect. The change in series resistance with light exposure may indicate a contact effect but does not change our conclusions about increased recombination in the active layer. Both the photocurrent spectral response and $J_{PC}(V)$ are measured at sufficiently low light intensity that the increased voltage drop at the contacts are negligible.

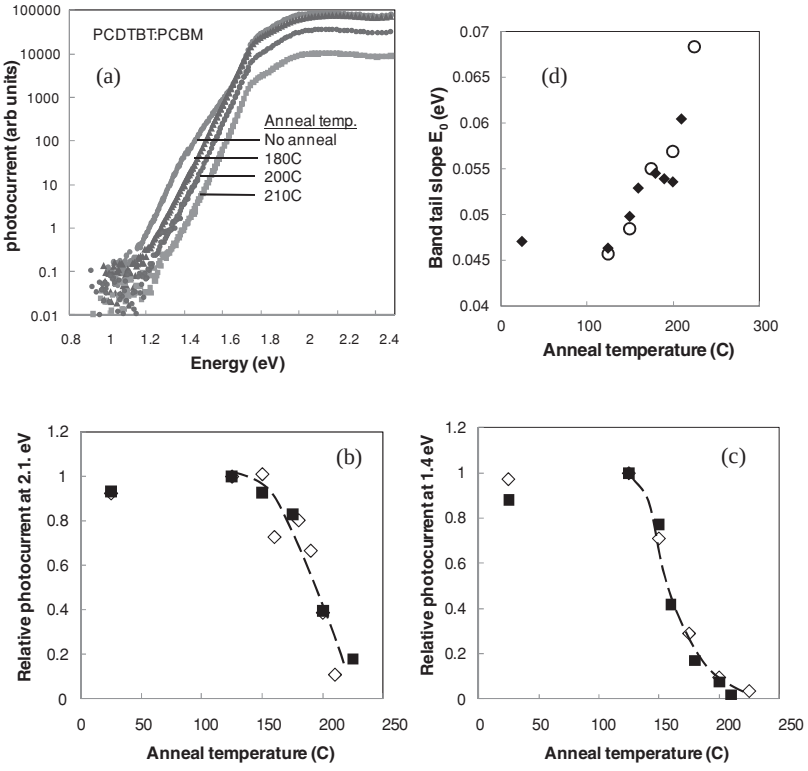


**Figure 5.** a) Spectral response of PCDTBT:PCBM after different annealing temperatures as indicated. b,c) Relative magnitude of the spectral response photocurrent for two samples, corresponding to b) bulk absorption at 2.1 eV and c) CT band-to-band absorption at 1.4 eV. d) Slope of the exponential optical absorption tail of the spectral response after different anneal temperatures for two PCDTBT:PCBM samples, measured from the spectral response data between 1.2 and 1.4 eV.

### 2.3. Thermal Annealing of PCDTBT:PCBM

There have been several studies of the effects of annealing BHJ solar cells, mostly for P3HT:PCBM.[13,29–35] Solar cells are usually annealed to optimize the cell performance, and the optimum anneal temperature is typically 100–150 °C.[34] Annealing to higher temperature is known to degrade the material and cell performance.[32] Diffusion and aggregation of the PCBM is observed by SEM so that the domain structure of the BHJ cell becomes more coarse.[31,33,35] An increase in the domain size is expected to degrade the cell performance because excitons created in the bulk will have a reduced probability of reaching the domain interface, corresponding to a reduction in $P_X$ in Equation 1.

PCDTBT:PCBM solar cells were annealed up to 200–225 °C to the point that the cells failed, presumably because they approach the melting point. **Figure 5**a shows examples of the spectral response data at various stages of annealing. There is little change at the lowest anneal temperature of 125 °C, which is expected since all the samples are pre-annealed after fabrication. In some cases there is a small increase in the peak spectral response, which may be the result of annealing some degradation mechanism that occurred during storage. Changes to the spectral response are observed in each of the four energy ranges indicated in Figure 1.

In the energy range above 2 eV, which corresponds to bulk absorption in the polymer and PCBM, the photocurrent changes little up to about 180 °C and then decreases at higher anneal temperatures, so that by 220C the response has decreased by about a factor 5. The relative change in spectral response at 2.1 eV is shown for two different samples in Figure 5b. In this and other data below, the changes are given relative to the data at the lowest anneal temperature of 125 °C, to remove any extraneous effects of the initial state of the sample.

The spectral response data of Figure 5a show that the CT absorption band also decreases with annealing but by a larger amount than the bulk absorption. The magnitude of CT band-to-band absorption is characterized by the magnitude of the spectral response at 1.4 eV, which is plotted in Figure 5c. The intensity has already dropped substantially after annealing at 175C and annealing to 220C results in a decrease at 1.4 eV by 20–50 times.

Changes also occur in the energy range $1.1 < E < 1.3$ eV corresponding to the exponential absorption edge of the CT

excitations. The data in Figure 5a indicate that the exponential tail becomes broader with annealing. An expanded plot of the spectral response data in the absorption tail region are given in the Supporting Information Figure S1. We fit this region of the spectral response to obtain the exponential slope and the values are shown for the same two samples in Figure 5d. The slope of the band tail increases by about 50% with annealing temperature, from 45 meV to about 70 meV. Beiley et al. observe a comparable increase in the band tail slope after thermal annealing in the same material system.[11]

Finally, no observable changes are found in the region of the spectral response below 1.1 eV which corresponds to optical transitions involving the deep trap states. Because of the reduction of the overall intensity of the CT band in the spectral response, the low energy band decreased below the noise level of the measurement for anneal temperatures above 170 °C. From the non-observation of this absorption band, we can only conclude that further annealing does not increase the relative intensity of this band more than the corresponding decrease in overall CT absorption strength.

**Figure 6** shows the $J_{PC}(V)$ data for one of the annealed PCDTBT:PCBM cells. There is a small increase in photocurrent with the lowest temperature anneals as was evident from the spectral response data, with the 150 °C anneal giving the highest current. At higher anneal temperatures, the $J_{PC}(V)$ curves flatten and the reverse bias current decreases. The charge collection model of Equation 2 provides a reasonable fit to the most of the data, but is less good at the high anneal temperatures, so the corresponding values of $S$ are more approximate. Figure 6b shows that the charge collection parameter decreases by about 10× as a result of annealing for the two samples measured, indicating an increase in the density of recombination centers of this amount. As discussed above there is no measureable increase in the relative value of the spectral response at 1 eV, suggesting that deep states are not the origin of the additional recombination.

Examples of the dark forward bias current are shown in **Figure 7**a for one sequence of thermal annealing. The series resistance is unchanged until an anneal temperature of about 200C and then increases rapidly just before the device fails. The ideality factor increases with the anneal temperature, as shown in Figure 7b. Although the trend is the same as for the light exposure case, the change in n is substantially smaller than is observed for light exposure, for the same change in $S$.

Since annealing changes the cell morphology, and a reduction in photogenerated carriers is observed, it is possible that annealing may change the structure such as to increase the contribution from geminate recombination. A test for geminate recombination was performed using a technique described previously,[18] but was found to be insignificant, as described in the Supporting Information.

### 2.3.1. Microstructure Effects of Thermal Annealing

The data show that a complex set of changes occurs with annealing. Two mechanisms can contribute to the changes in the magnitude of the spectral response in the bulk and CT band-to-band region. The coarsening of the domain structure reduces the number of excitons reaching the interface, and an increase in recombination can reduce the charge collection. The measured broadening of the band tails and associated drop in carrier mobility show that there are related changes in the electronic structure. The full set of measurements is able to separate out these different effects according to the following analysis.

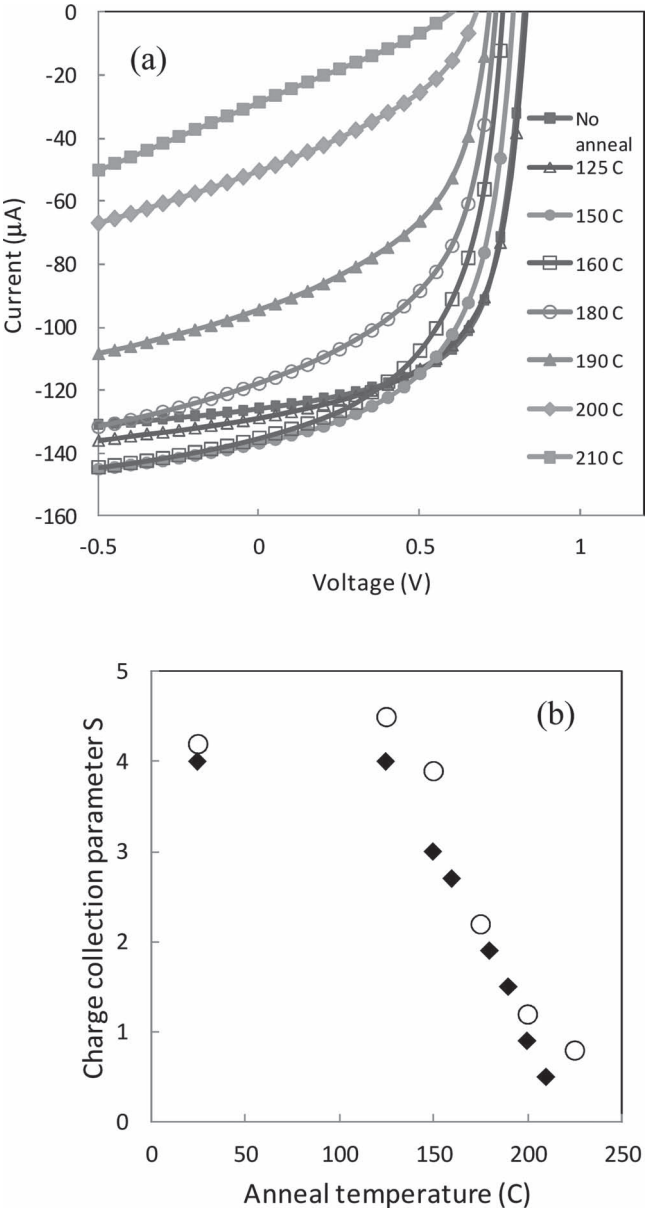


**Figure 6.** a) Bias dependence of the PCDTBT:PCBM steady state photocurrent $J_{PC}(V)$ after different anneal temperatures as indicated. b) Charge collection parameter $S$ obtained from the $J_{PC}(V)$ measurements for the annealing sequence of two similar samples.

From the discussion of Equation 1, the spectral response measured at short circuit and normalized to the incident light intensity is,

$$J_{PC}(E_{PH})/G = A_B(E_{PH})\,P_X\,J_{PC}(0)/J_{MAX} \quad (7)$$

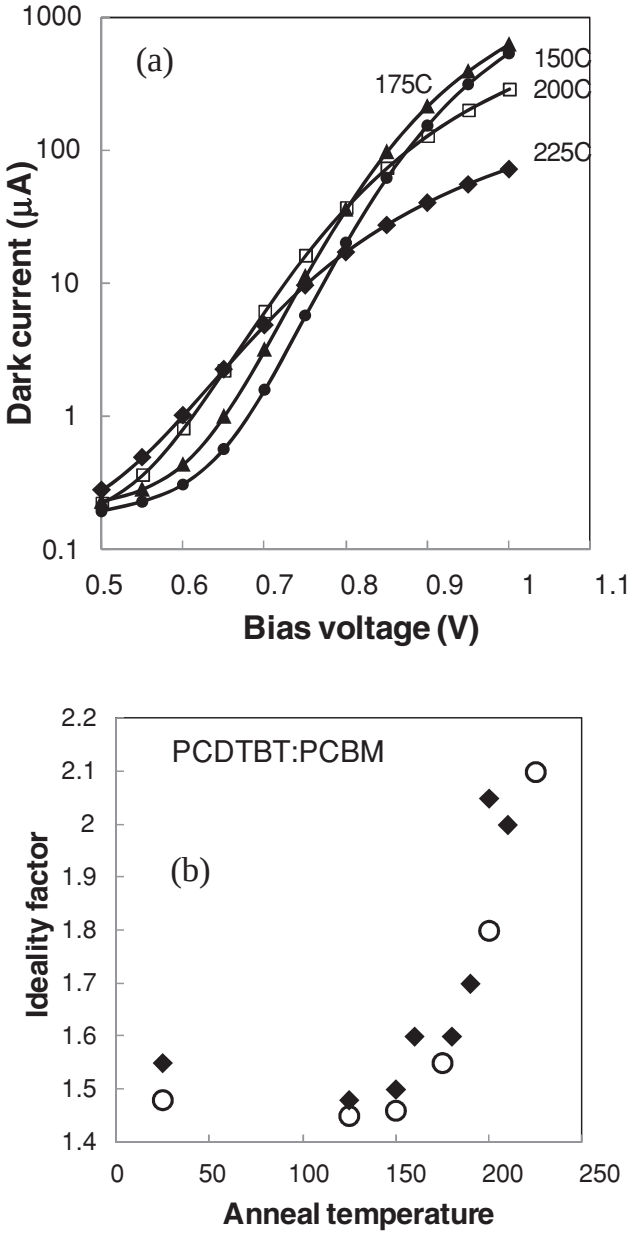


**Figure 7.** a) Dark forward bias current of PCDTBT:PCBM after different annealing temperatures. Points are data and lines are fits to Equation 4. b) Ideality factor obtained from dark current measurements for the annealing sequence of two samples.

The first step in the analysis is to correct the spectral response data for $J_{PC}(0)/J_{MAX}$ obtained from the fits of $J_{PC}(V)$ to Equation 2, thus providing a measurement of $A_B(E_{PH})P_X$. **Figure 8**a shows that the corrected magnitude of the spectral response decreases for both the bulk absorption region above 2 eV and interface absorption absorption region at 1.4 eV, but with a much larger decrease for the interface absorption.

The origin of the decrease in $A_BP_X$ must be different in the two energy regions. The bulk response ($E_{PH} > 2$ eV) contains the exciton diffusion parameter $P_X$ which is expected to decrease if the domain size increases. On the other hand, there is no reason for the overall bulk absorption to decrease, since the total volume of material is unchanged, and indeed the appearance of the films is unchanged until the device fails. Hence we attribute the reduction in the bulk absorption in the spectral response to an increase in the domain size, which is known to occur in annealed BHJ cells,[31,33] and the associated drop in the probability $P_X$ that the excitons reach the interface. In contrast, the interface absorption creates electron-hole pairs without requiring any exciton diffusion and so $P_X$ is unity. However, the interface absorption depends on the fraction of the material that makes up the interface region, and as the domain size increases this fraction will decrease. Ray and Alam have modeled the time and temperature dependence of the domain size growth.[35]

A model to estimate the relative magnitude of $A_BP_X$ for the bulk and interface absorption as a result of domain coarsening is constructed as follows. A cylindrical domain is assumed with radius $R_{TA}$ at anneal temperature $T_A$, and with a constant exciton diffusion length $R_X$. We also assume that the probability that the exciton diffuses a distance $R$ is,

$$p(R) = \exp(-R/R_X) \tag{8}$$

It is well known that the domains are irregular in shape and so this model is highly approximate, but is useful to estimate the expected trends. A simplified model calculates the probability of diffusing to the nearest point on the interface, which is $p(R_{TA}-y)$ for a point y from the center of the domain. There is a significant probability of diffusion to the opposite side of the domain when $R_X$ is large compared to the domain size, which is taken into account by calculating the probability of either event. A more accurate model would include diffusion in all directions, but the added complexity is not warranted. Integrating over the area of the domain cross section gives the probability that the exciton reaches the interface,

$$P_X = \frac{1}{\pi R_{TA}^2} \times \int_0^{R_{TA}} [p(R_{TA}-y) + p(R_{TA}+y) - p(R_{TA}-y)\,p(R_{TA}+y)] \times 2\pi y\,dy \tag{9}$$

For the case of the CT transitions, the absorption decreases as the domain size gets larger by a factor proportional to the surface to volume ratio. The same model of a cylindrical domain gives for the interface absorption $A_{BI}(T_A)$ at anneal temperature $T_A$, normalized to the unannealed value,

$$A_{BI}(T_A)/A_{BI}(0) = R_0/R_{TA} \tag{10}$$

Figure 8b compares the expected change in the magnitude of the photocurrent for the bulk and interface according to Equation 9 and 10. $R_X$ is set to be 2.5 times the initial radius, chosen so that the bulk probability for excitons to reach the interface in the initial state ($R_{TA} = R_0$) is about 95%, which is consistent with experiment in high quantum efficiency cells. The model shows that the interface absorption photocurrent

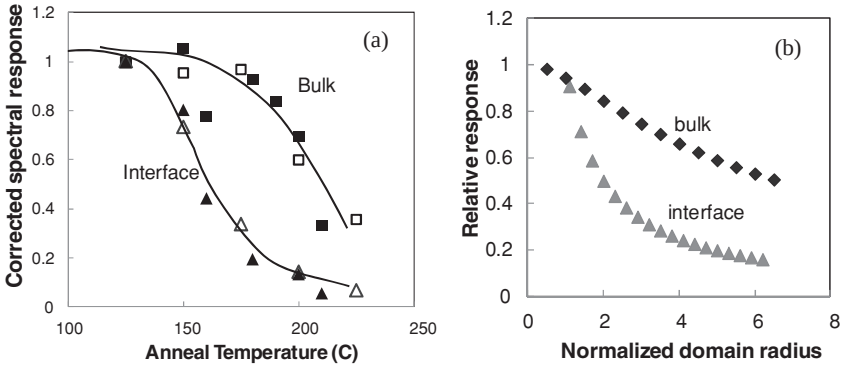


**Figure 8.** a) Magnitude of the spectral response after correction for the charge collection for the bulk transitions at 2 eV and the interface transitions at 1.4 eV. b) Calculated relative reponse of bulk and interface transitions based on the model for bulk and interface absorption with increasing domain size discussed in Section 2.3.1.

decreases much faster than the bulk absorption photocurrent, which agrees with the measurements in Figure 8a. The model predicts that the bulk absorption drops to ≈60% and the interface absorption to 20% of the unannealed value, when the domain size has increased by 5×, and this agrees roughly with the spectral response measurements at an anneal temperature of 200C. The spectral response data therefore are consistent with the reported coarsening of PCBM.[31,33]

### *2.3.2. Recombination Centers Resulting from Thermal Annealing*

Having separated out the effects related to the increase in domain size, we now consider how thermal annealing changes the recombination properties. Figure 6 shows a decrease in charge collection with annealing, from which we conclude that there is an increase in the density of recombination centers. The lack of observed intensity dependence of $J_{PC}(V)$ also shows that the recombination has first order kinetics. The charge collection parameter $S$, derived from the measurements of $J_{PC}(V)$, decreases with annealing by about a factor 10 (Figure 6b), suggesting a corresponding increase in recombination center density. Since we do not observe additional deep traps as measured by the spectral response below 1.1 eV, instead we consider the possibility that deep band tail states act as the recombination centers.

The data of Figure 5d and S1 (Supporting Information) show that the band tails do become increasingly broad with annealing and therefore there is an increase in the density of deep tail states. For example, an increase in the band tail slope from 45 meV to 60 meV results in a 15-fold increase in the density of states at a trap depth of 0.5 eV. The observed change in band tail slope is therefore consistent with the recombination centers being deep band tail states.

One expected consequence of the increased band tail slope is a decrease in the carrier mobility. Although the mobility cannot be measured over the full range of thermal anneal temperature because recombination increasingly dominates, the data in Figure S2 of the Supporting Information is sufficient to show that the mobility does decrease with annealing, consistent with the wider band tails. Another expected consequence of an increasing width of the band tails is an increase in the ideality factor which is also observed from the data in Figure 7. Modeling by Kirchartz et al. show that tail state recombination is consistent with both the illuminated and dark characteristics of P3HT:PCBM.[36] Giebink et al. also show that the ideality factor increases with band tail slope.[37] Hence both the mobility and dark current data support the evidence of a broadening band tail slope.

The measurement and analysis of thermal annealing therefore show that there are two distinct mechanisms involved in the solar cell response. Annealing increases the domain size such that the probability that excitons reach the interface decreases significantly, reducing the cell efficiency. A second effect is that for those excitons that split at the interface to create mobile carriers, the recombination rate increases and so the cell fill factor and efficiency are further reduced. Section 3 describes a specific model relating the band tail slope to the recombination.

### 2.4. PCDTBT:PCBM with Doped Fullerenes

Samples of PCDTBT:PCBM were fabricated doped with the different fullerene $PC_{84}BM$ which is known to have a lower LUMO level than PCBM and therefore is expected to introduce dopant states in the PCBM band gap, below the LUMO level. Cowan et al. showed an increase in recombination in this material system,[38] and earlier Mandoc et al. reported similar effects with a different acceptor dopant.[39] Samples were studied with doping levels of 1.8%, 6% and 12% of $PC_{84}BM$. The data for the spectral response and $J_{PC}(V)$ are shown in **Figure 9** and compared to an undoped control sample. The spectral response data is normalized to the peak value and the normalization factor is consistent with the estimated $J_{PC}(0)/J_{MAX}$ obtained from the $J_{PC}(V)$ measurements (see Equation 7). After scaling, the above gap absorption is unchanged and the interface absorption above 1.4 eV is only slightly modified, indicating that there is minimal change in the morphology of the films with doping. The primary change is an additional optical transition in the energy range $1.0 < E < 1.4$ eV which evidently originates from the doping. The inset to Figure 9a shows that the strength of this signal in the spectral response increases proportionally with the doping level. The exponential absorption edge is shifted to lower energy, but there is no significant change in the slope of the exponential absorption tail. The low energy absorption is weak and shows no sign of a significant increase with doping.

The $J_{PC}(V)$ data in Figure 9b shows a clear signature of increased recombination with increased doping, as previously reported.[38] With 1.8% doping, the charge collection parameter $S$ decreases by about a factor 5 and continues to decrease further at higher doping levels, although it is unchanged between 6 and 12% dopant. Evidently the doping introduces additional recombination centers. However, the shape of $J_{PC}(V)$ also changes with light intensity, more so than in the two previous cases of increased recombination. Figure 9c shows $J_{PC}(V)$ data for the 1.8% doping level for a variation of approximately 100×

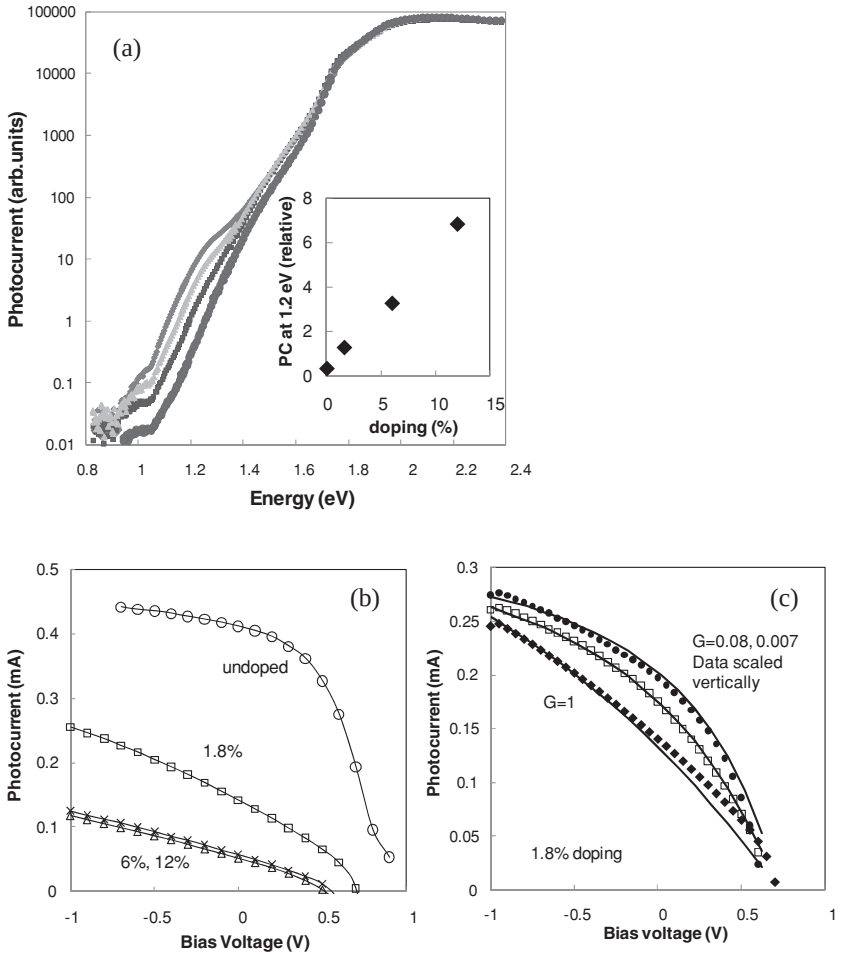


**Figure 9.** a) Spectral response data for undoped PCDTBT:PCBM and solar cells doped with $PC_{84}BM$. The inset plots the relative magnitude of the spectral response at 1.2 eV versus doping level. b) Steady state photocurrent measurements of $J_{PC}(V)$ for the doped and undoped samples at a fixed illumination level. c) $J_{PC}(V)$ data for the 1.8% sample at different illumination levels, $G$, with relative intensity as shown. The solid lines are a model based on a combination of first and second order recombination according to Equation 3.

the recombination properties. The spectral response has a shoulder at about 1.25 eV which is evidently due to transitions to dopant states. Since the transition energy is below that of the 1.4 eV interface band gap, the transition is most likely also at the domain interface, and is from the polymer HOMO to the dopant state. It seems unlikely that such a low energy transition within the bulk of the PCBM would generate photocurrent. The proposed density of states is therefore illustrated in **Figure 10**. The low energy exponential region of the additional spectral response component has about the same shape as the undoped material, from which we conclude that the dopant level is reasonably narrow in energy, as drawn in the inset to Figure 10b with a gaussian width of 40 meV. The optical absorption transition was modeled as the joint density of states of the polymer HOMO and the fullerene LUMO, as described previously.[14] Figure 10b shows the dopant distribution used in the model and the fit to the spectral response. The fit parameters can be varied slightly, but the result confirms that the dopant band is narrow and is 0.2–0.25 eV below the PCBM LUMO level, which is a bit smaller than the energy difference obtained from measurements of the LUMO for the two types of PCBM.[38]

The measurement of $J_{PC}(V)$ show that recombination increases, with a decrease in $S$ by 5× with the 1.8% doping level and a further decrease at the higher doping levels, as observed previously.[38] The exponential absorption tail to low energy is hardly changed by doping (Figure 9a), suggesting that there is no change in the polymer in light intensity. The data for the lower light levels are scaled vertically and the change of shape is obvious, indicating a significant component of higher order (i.e., bimolecular) recombination.

The $J_{PC}(V)$ data also show that the built-in potential drops from 0.85 eV at zero doping to 0.55 eV at the higher doping levels, presumably because the presence of the doping level below the PCBM LUMO reduces the built-in potential. From the evidence of the spectral response that the dopant states are the only new states introduced in the density of states distribution, these states must therefore be responsible for the additional recombination centers and the change in $J_{PC}(V)$.

Thus, the addition of $PC_{84}BM$ dopants to the PCDTBT:PCBM cell shows a clear change in both the spectral response and

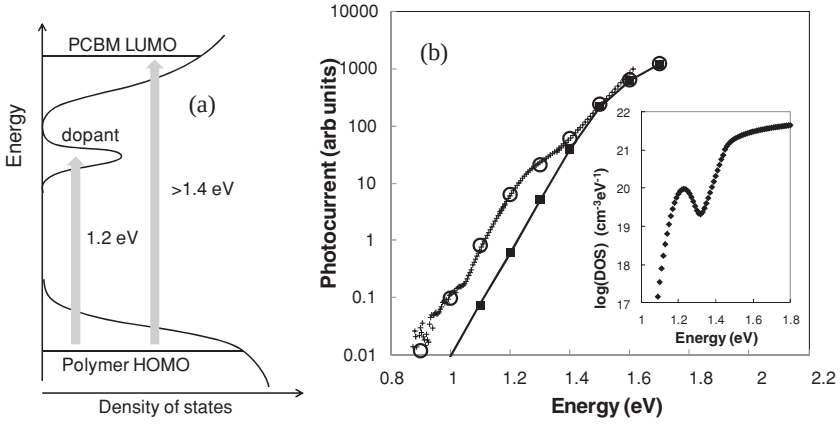


**Figure 10.** a) Proposed density of states model for the interface of the doped solar cell, indicating the dopant states near the PCBM LUMO, and the CT excitations. b) Calculated joint density of states (open circles) using the density of states model for the PCBM LUMO shown in the inset, compared to the measured spectral response for 12% doping. Square data points are the calculated joint density of states in the absence of doping.

disorder, as expected since only the PCBM is modified. We therefore conclude that the dopant states are the recombination centers. Absorption into the dopant band evidently excites photoconduction, otherwise it would not be observed in the spectral response. Excitation from the polymer LUMO to the dopant states creates a mobile hole which will contribute to the photocurrent. The electronic properties of these doped samples are described by Leong et al.[40]

The intensity dependence of the $J_{PC}(V)$ data (Figure 9c) suggest that the recombination has a significant component of second order recombination. This conclusion is confirmed by modeling based on Equation 3. The solid lines in Figure 9c show that the model provides a reasonably good fit to the data and certainly reproduces the change in shape of $J_{PC}(V)$. The fit required an increase in the first order recombination rate compared to the undoped control sample, as well as the introduction of the second order term. In general, recombination between the shallow dopant state and the polymer LUMO is expected to have more of a bimolecular character than a transition involving deep states, because the occupancy of the shallow states depends more on light intensity than does the occupancy of deep states below the quasi-Fermi energy. Hence the increased role of second order recombination is expected when the shallow dopants act as recombination centers. Previous measurements of this material system also shows a mixed recombination order in the doped cells for measurements made at open circuit.[38]

## 3. Discussion

The results described in this paper confirm that recombination occurs through localized trap states within the interface band gap. This adds to other evidence that relates the solar cell properties to Shockley-Read-Hall-type recombination.[5,41,42] Furthermore, the three different cases that are studied show that recombination can occur through different types of localized states depending on the circumstances. Thus light illumination induces states near the middle of the band gap, while thermal annealing broadens the band tails apparently without the additional midgap states, but both types of localized states act as recombination centers. A deep localized state of any origin has the potential to be a recombination center, depending mostly on the density and the capture cross-section. The doping study shows that more shallow states, only 0.2–0.25 eV from the valence band of the PCBM also increases the recombination. While the deeper recombination states have first order kinetics for our experimental conditions, the shallow dopant states show a contribution from second order recombination, as expected for states at or above the quasi-Fermi energies.

In each of the studies, recombination centers are added. Hence there remains a question of whether recombination in the pristine solar cells is also limited by localized states and if so, of which type. The spectral response measurements of Figure 1b show that the pristine cell (subjected to only limited illumination) has a measurable density of deep states, as measured by the low energy spectral response. However, the relation between 1/S and the deep state density in Figure 4 suggest that a component of recombination remains even if the deep states are absent.

For recombination through low energy states of an exponential band tail, the density of tail states with larger binding energy than $E_B$ is,

$$N_T(E > E_B) = N_o E_0 \exp(-E_B/E_0) \quad (11)$$

Assuming that these tail states are the recombination centers, we set $N_T$ proportional to $1/S$ according to Equation 5, so that,

$$\ln(1/S) = \text{const} - E_B/E_0 \quad (12)$$

**Figure 11**a replots the thermal annealing data of Figure 5a and 6b in this form. Although there is considerable scatter in the data, the trend is consistent with Equation 12 and the

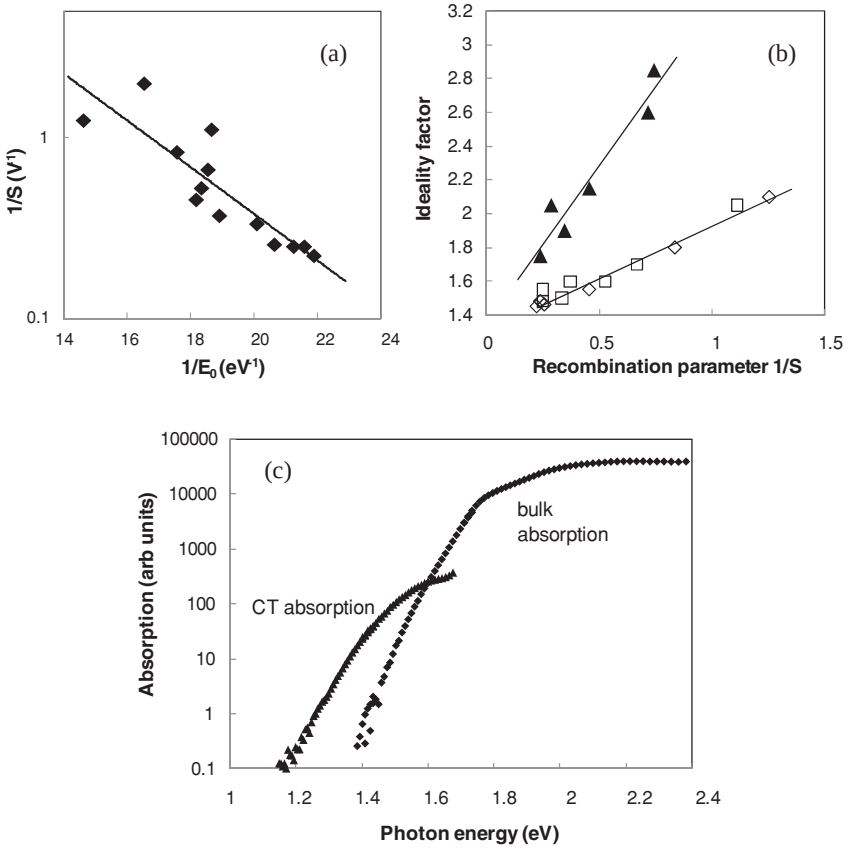


**Figure 11.** a) Plot of 1/S versus $1/E_0$ for the two thermally annealed samples showing the relation described by Equation 12. b) Plot of ideality factor versus recombination state parameter $1/S$ for prolonged illumination (solid symbols) and the two thermal annealed samples (open symbols). c) Separate bulk and CT absorption bands derived from the spectral response data of thermally annealed PCDTBT:PCBM, assuming that the measurements are the superposition of two bands of fixed spectral shape.

slope indicates that the active band tails states are deeper than $E_B \approx 0.3$ eV. The initial cell data are included in Figure 11 and hence suggest that band tail states are the main recombination center in pristine PCDTBT:PCBM with deeper mid-gap states being a secondary component. We therefore conclude that the as-received cells operate with the same recombination processes as the degraded cells. The relative contribution of band tail and deep states is presumably specific to the particular type of cell and perhaps to the specific details of the fabrication.

The relation between the ideality factor and the density of recombination centers for prolonged illumination and thermal annealing can be extracted from Figure 3, 4, 6b, and 7b, and the result is shown in Figure 11b. The data lie on two different trend lines, with the mid-gap states corresponding to a larger change in ideality factor than the band tail states for the same value of $1/S$. It is reasonable to expect that band tails states and deep traps will have a different influence on the recombination rates and the dark forward current. Such relationships might prove useful in the future to identify the character of unknown recombination centers.

Although we can determine the character of the recombination centers, these experiments provide no definitive information about their origin. It seems likely that the broader band tails induced by thermal annealing are the result of increased disorder of the materials, but since the annealing is done in air, impurities cannot be ruled out. Similarly the light induced states, and particularly the observed saturation, suggest an impurity effect, but intrinsic states also cannot be ruled out. Recent studies of X-ray radiation damage using the same methodology leads to specific proposals for the recombination centers.[43]

Finally the data provide an additional insight into the optical absorption of the component materials of the BHJ cell. Thermal annealing changes the relative contribution of the bulk and the CT absorption and allows a deconvoution of the two bands. A simple model assumes that the two bands do not change their spectral shape with annealing and only the intensity changes, so that the spectrum is a superposition of the two components. Two measurements at different anneal temperatures therefore allows the bands to be separated and the result is shown in Figure 11c. The bulk absorption band drops off relatively steeply at low energy and has an approximately exponential slope of about 30 meV. This result is consistent with lowest energy bulk absorption being attributed to PCBM, and PCBM has been measured to have a band tail slope of about 30 meV.[44] Obtaining the high energy region of the CT absorption band is more challenging because it is masked by the much more absorbing bulk. To the extent that the separation can be made, the CT band flattens above the CT energy gap as expected from the joint density of states model.

## 6. Conclusions

These studies show that the localized state distribution of PCDTBT:PCBM solar cells can be modified by prolonged illumination, thermal annealing or doping. In each case localized states of a different character are introduced and can be quatified by measurements of the spectral response. Photoconductivity and dark conductivity show that the additional localized states act as recombination centers. In each case the measurements show a direct correlation between the introduction of localized states and the presence of recombination centers. We therefore confirm that localized band gap states are the dominant recombination center in BHJ solar cells.

Prolonged illumination introduces localized states near the middle of the interface band gap while thermal annealing introduces additional band tails states and fullerene doping causes shallow states near the fullerene LUMO. Each of these different types of state act as recombination centers with slightly different properties.

## 7. Experimental Section

*Spectral Response*: The photoconductivity spectral response experiment used a 0.25 m grating spectrometer with a halogen light source. The measurements were performed with zero bias voltage (i.e., short circuit conditions) with a 9 kohm load resistor, which was increased to 30 kohm for some weak signals. The voltage across the load was measured with a lock-in amplifier with the monochromatic illumination source chopped at 230 Hz. Cut-off filters at 450, 715 and 850 nm reduce the scattered light sufficiently to measure signals with magnitude ~$10^{-7}$ of the peak signal, and the suppression of scattered light was confirmed by measurements with an infrared absorbing filter. The incident light power was measured with a calibrated silicon photodiode for data at wavelengths below 1100 nm and a Ge photodiode for the longer wavelengths, and the spectrum was normalized to the power.

*Dark and Photocurrent*: The voltage dependence of the photocurrent was measured using a white light source from a fiber-optic microscope illuminator chopped at 70 Hz and the current across an 11 ohm load resistor was measured with a lock-in amplifier. The use of lock-in techniques automatically subtracted the dark current. Neutral density filters in the optical path provided illumination levels differening by about a factor 100. The highest light intensity was significantly below 1-sun equivalent so that contributions from second order recombination processes were reduced. The dark current was measured with a Keithley 6487 picoammeter, which also provided the source voltage.

*Transient Photoconductivity*: A nitrogen pulsed dye laser operating at 520 nm with a repetition rate of about 1 Hz was used for the transient photocurrent measurements. The photocurrent was measured on a Tektronix digital oscilloscope from the voltage across a 11 ohm load resistor, and averaged over up to 128 repetitions. The excitation was kept sufficiently small that the charge extracted is much less than $CV$, where $C$ is the device capacitance, and the voltage across the load resistor was less than 100 mV.

*Light Exposure and Thermal Annealing*: Extended light exposure used a fiber-optic microscope illuminator with a halogen light source and a lens to focus the light. No attempt was made to quantify and characterize the illumination accurately. The measurements were initially made at a light intensity of about 200 mW/cm$^2$ and the intensity was later increased to about 600 mW/cm$^2$ to accelerate the changes. The total illumination time was about 6 days. The illuminated area was kept small (≈0.2 cm$^2$) to minimize heating. Moderate heating of the substrate occurred, but was not measured.

For thermal annealing experiments, the solar cells were annealed in an ambient atmosphere oven for 1 h and cooled in ambient before measuring. The cells were initially fabricated and annealed to give the optimum solar cell response, and were subsequently stored in a nitrogen atmosphere for several months. Some of the devices were used in earlier experimental measurements.

## Supporting Information

Supporting Information is available from the Wiley Online Library or from the author.

## Acknowledgements

The authors are grateful to C. Paulson for technical assistance. The work done at UCSB was supported by the Air Force Office of Scientific Research (FA9550-11-1-0063).

Received: January 4, 2012
Revised: May 15, 2012
Published online: July 3, 2012

[1] V. D. Mihailetchi, L. J. A Koster, J. C Hummelen, P. W. M. Blom, *Phys. Rev. Lett.* **2006**, *93*, 216601.
[2] J. Szmytowski, *Semicond. Sci. Technol.* **2010**, *25*, 015009.
[3] H. H. P. Gommans, M. Kemerink, J. M. Kramer, R. A. J. Janssen, *Appl. Phys. Lett.* **2005**, *87*, 122104.
[4] T. Kirchatz, B. E. Pieters, K. Taretto, U. Rau, *J. Appl. Phys.* **2008**, *104*, 094513.
[5] R. A. Street, M. Schoendorf, A. Roy, J. H. Lee, *Phys. Rev. B* **2010**, *81*, 205307.
[6] R. A. Street, S. CowanA. J. Heeger, *Phys. Rev. B* **2010**, *82*, 121301.
[7] a) W. L. Kalb, S. Haas, C. Krellner, T. Mathis, B. Batlogg, *Phys. Rev. B.* **2010**, *81*, 155315; b) W. L. Kalb, B. Batlogg, *Phys. Rev. B.* **2010**, *81*, 035327.
[8] A. J. Campbell, D. D. C. Bradley, D. G. Lidzey, *J. Appl. Phys.* **1997**, *82*, 6326.
[9] J. Nelson *Phys. Rev. B* **2003**, *67*, 155209.
[10] Z. Chiguvare, V. Dyakonov, *Phys. Rev. B* **2004**, *70*, 235207.
[11] Z. M. Beiley, E. T. Hoke, R. Noriega, J. Dacuna, G. F. Burkhard, J. A. Bartelt, A. Salleo, M. F. Toney, M. D. McGehee, *Adv. Energy Mater.* **2011**, *1*, 954.
[12] C. G. Shuttle, N. D. Treat, J. D. Douglas, J. M. J. Frechet, M. L. Chabinyc, *Adv. Energy Mater.* **2012**, *2*, 111.
[13] S. H. Park, A. Roy, S. Beaupre, N. Coates, J. S. Moon, D. Moses, M. Leclerc, K. Lee, A. J. Heeger, *Nat. Photonics* **2009**, *3*, 297.
[14] R. A. Street, K. W. Song J. E. Northrup, S. Cowan, *Phys Rev. B* **2011**, *83*, 165207.
[15] R. A. Street, *Phys. Rev. B* **2011**, *84*, 075208.
[16] J. Lee, K. Vandewal, S. R. Yost, M. E. Bahlke, L. Goris, M. A. Baldo, J. V. Manca, T. Van Voorhis, *J. Am. Chem. Soc.* **2010**, *132*, 11878.
[17] K. Vandewal, K. Tvingstedt, A. Gadisa, O. Inganäs, J. V. Manca, *Phys. Rev. B.* **2010**, *81*, 125204.
[18] R. A. Street, *Phys. Rev. B* **2010**, *82*, 207302.
[19] J. H. Lee, S. Cho, A. Roy, H.-T. Jung, A. J. Heeger, *Appl. Phys. Lett.* **2010**, *96*, 163303.
[20] Priciples of Semiconductor Devices, http://ecee.colorado.edu/~bart/book/book/chapter4/ch4_4.htm (accessed May 2012).
[21] M. O. Reese, A. M. Nardes, B. L. Rupert, R. E. Larsen, D. C. Olson, M. T. Lloyd, S. E. Shaheen, D. S. Ginley, G. Rumbles, N. Kopidakis, *Adv. Funct. Mater.* **2010**, *20*, 3476.
[22] C. L. Huisman, A. Goossens, J. Schoonman, *J. Phys. Chem. B* **2002**, *106*, 10578.
[23] C. H. Peters, I. T. Sachs-Quintana, W. R. Mateker, T. Heumueller, J. Rivnay, R. Noriega, Z. M. Beiley, E. T. Hoke, A. Salleo, M. D. McGehee, *Adv. Mater.* **2011**, *24*, 663.
[24] M. O. Reese, A. J. Morfa, M. S. White, N. Kopidakis, S. E. Shaheen, G. Rumbles, D. S. Ginley, *Sol. Energy Mater. Sol. Cells* **2008**, *92*, 746.
[25] L. Goris, A. Poruba, L. Hodakova, M. Vanacek, K. Haenen, M. Nesladek, P. Wagner, D. Vandezander, L. De Schepper, J. V. Manca, *Appl. Phys. Lett.* **2006**, *88*, 052113.
[26] R. A. Street, K. W. Song, S. Cowan, *Org. Electron.* **2011**, *12*, 244.
[27] R. A. Street, *Philos. Mag.* **1984**, *49*, L15.
[28] R. A. Street, M. Hack, *MRS Symp. Proc.* **1991**, *219*, 135.
[29] M. Campoy-Quiles, T. Ferenczi, T. Agostinelli, P. G. Etchegoin, Y. Kim, T. D. Anthopoulos, P. N. Stavrinou, D. D. C. Bradley, J. Nelson *Nat. Mater.* **2008**, *7*, 158.
[30] B. Conings, S. Bertho, K. Vandewal, A. Senes, J. D'Haen, J. Manca, R. A. J. Janssen, *Appl. Phys. Lett.* **2010**, *96*, 163301.
[31] B. Watts, W. J. Belcher, L. Thomsen, H. Ade, P. C. Dastoor, *Macromolecules* **2009**, *42*, 8392.
[32] J. M. Warman, M. P. de Haas, T. D. Anthopoulos, D. M. de Leeuw, *Adv. Mater.* **2006**, *18*, 2294.
[33] T. Agostinelli, S. Lilliu, J. G. Labram, M. Campoy-Quiles, M. Hampton, E. Pires, J. Rawle, O. Bikondoa, D. D. C. Bradley, T. D. Anthopoulos, J. Nelson, J. E. Macdonald, *Adv. Funct. Mater.* **2011**, *21*, 1701.
[34] W. Ma, C. Yang, X. Gong, K. Lee, A. J. Heeger, *Adv. Funct. Mater.* **2005**, *15*, 1617.
[35] B. Ray, M. A. Alam, *Appl. Phys. Lett.* **2011**, *99*, 033303.
[36] T. Kirchartz, B. E. Pieters, J. Kirkpatrick, U. Rau, J. Nelson, *Phys. Rev. B* **2011**, *83*, 115209.
[37] N. C. Giebink, G. P. Wiederrecht, M. R. Wasielewski, S. R. Forrest, *Phys. Rev. B* **2010**, *82*, 155305.
[38] S. R. Cowan, W. L. Leong, N. Banerji, G. Dennier, A. J. Heeger, *Adv. Funct. Mater.* **2011**, *21*, 3083.
[39] M. M. Mandoc, F. B. Kooistra, J. C. Hummelen, B. de Boer, P. W. M. Blom, *Appl. Phys. Lett.* **2007**, *91*, 263505.
[40] W. L. Leong, G. Hernandez-Sosa, S. R. Cowan, D. Moses, A. J. Heeger, *Adv. Mater.* **2012**, *24*, 2273.
[41] G. Garcia-Belmonte, J. Bisquert, *Appl. Phys. Lett.* **2010**, *96*, 113301.
[42] L. Tsabari, N. Tessler, *J. Appl. Phys.* **2011**, *109*, 064501.
[43] R. A. Street, J. E. Northrup, B. S. Krusor, *Phys. Rev. B* **2012**, *85*, 205211.
[44] A. Salleo, unpublished.